519

12

Yield and Fracture Criteria

12-1. Introduction

From the preceding study of the text, it should be apparent that in numerous technical problems, the state of stress and strain at critical points may be very complex. Idealized mathematical procedures for determining those states, as well as their transformations to different coordinates, are available. However, the precise response of real materials to such stresses and strains defies accurate formulations. A number of questions remain unsettled and are part of an active area of materials research. As yet, no comprehensive theory can provide accurate predictions of material behavior under the multitude of static, dynamic, impact, and cyclic loading, as well as temperature effects. Only the classical idealization of yield and fracture criteria for materials is discussed here. Of necessity, they are used in the majority of structural and machine designs. These strength theories are structured to apply to particular classes of materials. The two most widely accepted criteria for the onset of inelastic behavior (yield) for ductile materials under combined stresses are discussed first. This is followed by presentation of a fracture criterion for brittle materials. It must be

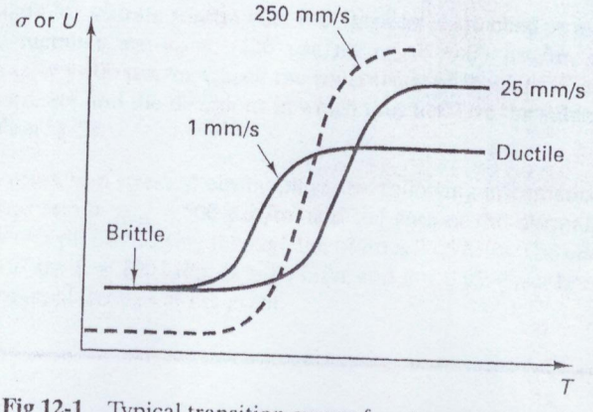

Fig 12-1 Typical transition curves for stress or energy to fracture versus temperature for low-carbon steel (adapted from Manjoine, see footnote 1).

emphasized that, in classifying materials in this manner, one refers to the brittle or ductile state of the material, as this characteristic is greatly affected by temperature as well as by the state of stress itself. For example, some low-carbon steels, below their transition temperatures of about 10°C (+50°F), become brittle, lose their excellent ductile properties,[1] and behave like different materials (Fig. 12-1). Experimental evidence shows that the transition temperature is sensitive to the rate of load application. For the faster rates, the transition temperature tends to occur at a higher temperature.

Most of the information on yielding and fracture of materials under the action of biaxial stresses comes from experiments on thin-walled cylinders. A typical arrangement for such an experiment is shown in Fig. 12-2. The ends of the thin-walled cylinder of the material being investigated are closed by substantial caps. This forms the hollow interior of a cylindrical pressure vessel. By pressurizing the available space until the yielding or bursting occurs, the elements of the wall are subjected to biaxial stresses of a constant ratio $\sigma_1/\sigma_2 = 2$. By applying an additional tensile force P to the caps, the σ_2 stress is increased to any predetermined amount $\sigma_2 + \sigma''$. By applying a comprehensive force, the σ_2 stress can be minimized or eliminated. Actual compressive stress in the longitudinal direction is undesirable, as the tube may buckle. By maintaining a fixed ratio between the principal stresses until the failure point is reached, the desired data on a material are obtained. Analogous experiments with tubes simultaneously subjected to torque, axial force, and pressure are also used. An interpretation of these data, together with all other related experimental evidence,

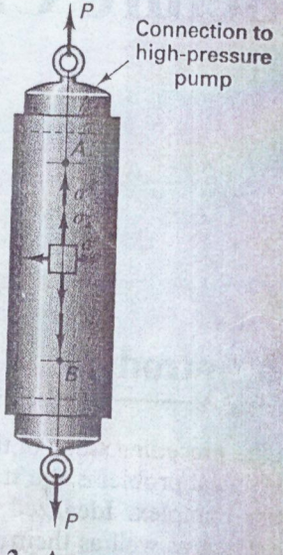

Fig. 12-2 Arrangement for controlled ratios of principal stresses.

[1]See M. J. Manjoine, "Influence of rate of strain and temperature on yield stresses of mild steel," *J. Appl. Mech., ASME* (1944), A211–218.

including the simple tension tests, permits a formulation of theories of failure for various materials subjected to combined stresses.

12-2. Maximum Shear-Stress Theory

The maximum shear-stress theory,[2] or simply the maximum shear theory, results from the observation that in a *ductile* material, slip occurs during yielding along critically oriented planes. This suggests that the maximum shear stress plays the key role, and it is assumed that yielding of the material depends only on the maximum shear stress that is attained within an element. Therefore, whenever a certain critical value τ_{cr} is reached, yielding in an element commences.[3] For a given material, this value usually is set equal to the shear stress at yield in simple tension or compression. Hence, according to Eq. 11-9, if $\sigma_x = \pm\sigma_1 \neq 0$ and $\sigma_y = \tau_{xy} = 0$,

$$\tau_{max} \equiv \tau_{cr} = \left| \pm \frac{\sigma_1}{2} \right| = \frac{\sigma_{yp}}{2} \tag{12-1}$$

which means that if σ_{yp} is the yield-point stress found, for example, in a simple tension test, the corresponding maximum shear stress is half as large. This conclusion also follows easily from Mohr's circle of stress.

In applying this criterion to a biaxial plane stress problem, two different cases arise. In one case, the signs of the principal stresses σ_1 and σ_2 are the same. Taking them, for example, to be tensile, as in Fig. 12-3(a), and setting $\sigma_3 = 0$, the resulting Mohr's principal stress circles are as shown in Fig. 12-3(b). Here the maximum shear stress is of the same magnitude as would occur in a simple uniaxial stress, as in Figs. 12-3(a) and (c). Therefore, if $|\sigma_1| > |\sigma_2|$, then according to Eq. 12-1, $|\sigma_1|$ must not exceed σ_{yp}. Similarly, if $|\sigma_2| > |\sigma_1|$, $|\sigma_2|$ must not be greater than σ_{yp}. Therefore, the criteria corresponding to this case are

$$\boxed{|\sigma_1| \leq \sigma_{yp}} \quad \text{and} \quad \boxed{|\sigma_2| \leq \sigma_{yp}} \tag{12-2}$$

The second case is considered in Fig. 12-3(d)–(f), where the signs of σ_1 and σ_2 are opposite, and $\sigma_3 = 0$. The largest Mohr's circle passes through σ_1 and σ_2, and the maximum shear stress $\tau_{max} = (|\sigma_1| + |\sigma_2|)/2$. The alternative possible slip planes are identified in Fig. 12-3(d) and (f). This maximum

[2] This theory appears to have been originally proposed by C. A. Coulomb in 1773. In 1868, Tresca presented the results of his work on the flow of metals under great pressures to the French Academy. Now this theory often bears his name.

[3] In single crystals, slip occurs along preferential planes and in preferential directions. In studies of this phenomenon, the effective component of the shear stress causing slip must be carefully determined. Here it is assumed that because of the random orientation of numerous grains, the material has isotropic properties, and so by determining τ_{max}, one finds the critical shear stress.

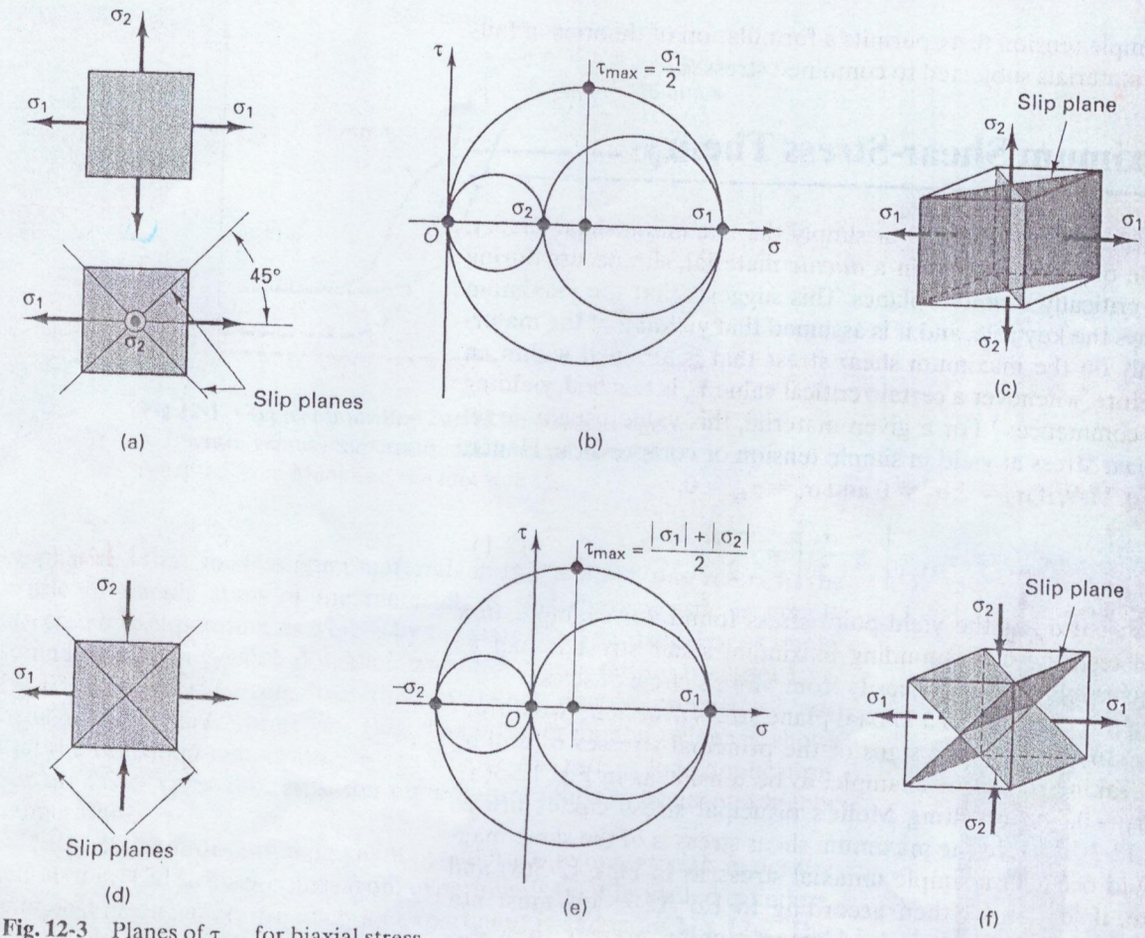

Fig. 12-3 Planes of τ_{max} for biaxial stress.

shear stress cannot exceed the shear yield criterion in simple tension (i.e., $\tau_{max} \leq \sigma_{yp}/2$). Hence,

$$\left| \pm \frac{\sigma_1 - \sigma_2}{2} \right| \leq \frac{\sigma_{yp}}{2} \tag{12-3}$$

or, for impending yield,

$$\frac{\sigma_1}{\sigma_{yp}} - \frac{\sigma_2}{\sigma_{yp}} = \pm 1 \tag{12-4}$$

A plot of this equation gives the two sloping lines shown in Fig. 12-4. Dividing Eqs. 12-2 by σ_{yp} puts them into the same form as Eq. 12-4. These

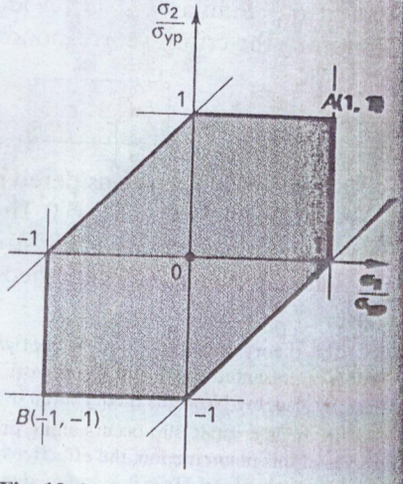

Fig. 12-4 Yield criterion based on maximum shear stress.

modified equations, $\sigma_1/\sigma_{yp} = \pm 1$ and $\sigma_2/\sigma_{yp} = \pm 1$, plot, respectively, in Fig. 12-4 as two vertical and two horizontal lines. Then, by treating σ_1/σ_{yp} and σ_2/σ_{yp} as coordinates of a point in this principal stress space, some important conclusions can be reached.

If a point defined by σ_1/σ_{yp} and σ_2/σ_{yp} falls on the hexagon shown in Fig. 12-4, a material begins and continues to yield. No such stress points can be outside the hexagon because one of the three yield criteria equations given before for perfectly plastic material would be violated. The stress points falling within the hexagon indicate that a material behaves elastically.

Note that, according to the maximum shear theory, if hydrostatic tensile or compressive stresses are added (i.e., stresses such that $\sigma_1' = \sigma_2' = \sigma_3'$), no change in the material response is predicted. Adding these stresses merely shifts the Mohr's circles of stress along the σ-axis, and τ_{max} remains the same. Also note that since the maximum shear stresses are defined on planes irrespective of material directional properties, it is implicit that the material is *isotropic*.

The derived yield criterion for perfectly plastic material is often referred to as the *Tresca yield condition* and is one of the widely used laws of plasticity.

12-3. Maximum Distortion-energy Theory

Another widely accepted criterion of yielding for *ductile* isotropic materials is based on energy concepts.[4] In this approach, the total elastic energy is divided into two parts: one associated with the volumetric changes of the material, and the other causing shear distortions. By equating the shear distortion energy at yield point in simple tension to that under combined stress, the yield criterion for combined stress is established.

In order to derive the expression giving the yield condition for combined stress, the procedure of resolving the general state of stress must be employed. This is based on the concept of superposition. For example, it is possible to consider the stress tensor of the three principal stresses—σ_1, σ_2, and σ_3—to consist of two additive component tensors. The elements of one component tensor are defined as the mean "hydrostatic" stress:

$$\bar{\sigma} = \frac{\sigma_1 + \sigma_2 + \sigma_3}{3} \tag{12-5}$$

[4] The first attempt to use the total energy as the criterion of yielding was made by E. Beltrami of Italy in 1885. In its present form, the theory was proposed by M. T. Huber of Poland in 1904 and was further developed and explained by R. von Mises (1913) and H. Hencky (1925), both of Germany and the United States.

The elements of the other tensor are $(\sigma_1 - \bar{\sigma})$, $(\sigma_2 - \bar{\sigma})$, and $(\sigma_3 - \bar{\sigma})$. Writing this in matrix representation, one has

$$\begin{pmatrix} \sigma_1 & 0 & 0 \\ 0 & \sigma_2 & 0 \\ 0 & 0 & \sigma_3 \end{pmatrix} = \begin{pmatrix} \bar{\sigma} & 0 & 0 \\ 0 & \bar{\sigma} & 0 \\ 0 & 0 & \bar{\sigma} \end{pmatrix} + \begin{pmatrix} \sigma_1 - \bar{\sigma} & 0 & 0 \\ 0 & \sigma_2 - \bar{\sigma} & 0 \\ 0 & 0 & \sigma_3 - \bar{\sigma} \end{pmatrix} \quad (12\text{-}6)$$

This resolution of the general state of stress is shown schematically in Fig. 12-5. The special case of resolving the uniaxial state of the stress in the figure has been carried a step further. The sum of the stresses in Fig. 12-5(f) and (g) corresponds to the last tensor of Eq. 12-6.

For the three-dimensional state of stress, the Mohr's circle for the first tensor component of Eq. 12-6 degenerates into a point located at $\bar{\sigma}$ on the σ-axis. Therefore, the stresses associated with this tensor are the same in every possible direction. For this reason, this tensor is called the *spherical stress tensor.* Alternatively, from Eq. 5-23, which states that dilatation of an elastic body is proportional to $\bar{\sigma}$, this tensor is also called the *dilatational stress tensor.*

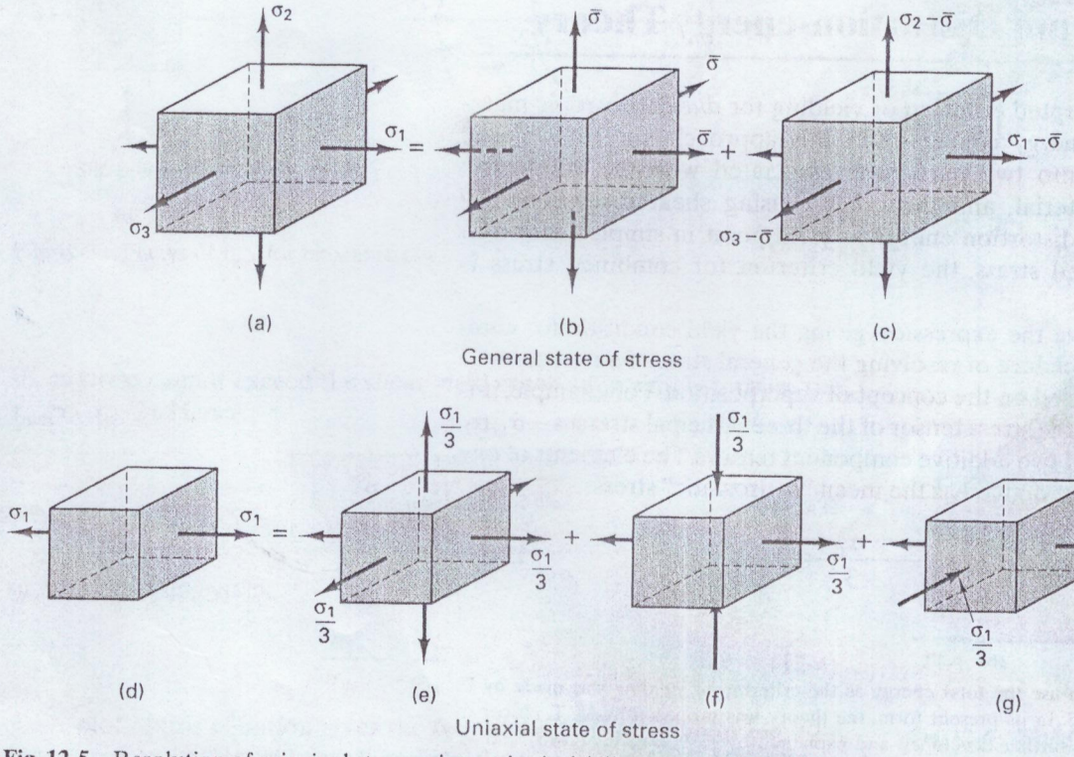

Fig. 12-5 Resolution of principal stresses into spherical (dilatational) and deviatoric (distortional) stresses.

The last tensor of Eq. 12-6 is called the *deviatoric* or *distortional stress tensor*. A good reason for the choice of these terms may be seen from Fig. 12-5(f) and (g). The state of stress consisting of tension and compression on the mutually perpendicular planes is equivalent to pure shear stress. The latter system of stresses is known to cause no volumetric changes in isotropic materials, but instead distorts or deviates the element from its initial cubic shape.

Having established the basis for resolving or decomposing the state of stress into dilatational and distortional components, one may find the strain energy due to distortion. For this purpose, first the strain energy per unit volume (i.e., strain density) for a three-dimensional state of stress must be found. Since this quantity does not depend on the choice of coordinate axes, it is convenient to express it in terms of principal stresses and strains. Thus, generalizing Eq. 3-13 for three dimensions using superposition, one has

$$U_O = U_{\text{total}} = \frac{1}{2}\sigma_1\varepsilon_1 + \frac{1}{2}\sigma_2\varepsilon_2 + \frac{1}{2}\sigma_3\varepsilon_3 \qquad (12\text{-}7)$$

where, by substituting for strains, Eqs. 5-14, expressed in terms of principal stresses, after simplifications, become

$$U_{\text{total}} = \frac{1}{2E}(\sigma_1^2 + \sigma_2^2 + \sigma_3^2) - \frac{\nu}{E}(\sigma_1\sigma_2 + \sigma_2\sigma_3 + \sigma_3\sigma_1) \qquad (12\text{-}8)$$

The strain energy per unit volume due to the dilatational stresses can be determined from this equation by first setting $\sigma_1 = \sigma_2 = \sigma_3 = p$, and then replacing p by $\bar{\sigma} = (\sigma_1 + \sigma_2 + \sigma_3)/3$. Thus,

$$U_{\text{dilatation}} = \frac{3(1-2\nu)}{2E}p^2 = \frac{1-2\nu}{6E}(\sigma_1 + \sigma_2 + \sigma_3)^2 \qquad (12\text{-}9)$$

By substracting Eq. 12-9 from Eq. 12-8, simplifying, and noting from Eq. 5-21 that $G = E/2(1+\nu)$, one finds the distortion strain energy for combined stress:

$$U_{\text{distortion}} = \frac{1}{12G}[(\sigma_1 - \sigma_2)^2 + (\sigma_2 - \sigma_3)^2 + (\sigma_3 - \sigma_1)^2] \qquad (12\text{-}10)$$

According to the basic assumption of the distortion-energy theory, the expression of Eq. 12-10 must be equated to the maximum elastic distortion energy in simple tension. The latter condition occurs when one of the principal stresses reaches the yield point, σ_{yp}, of the material. The distortion strain energy for this is $2\sigma_{yp}^2/12G$. Equating this to Eq. 12-10 after minor simplifications, one obtains the basic law for yielding of an ideally plastic material:

$$\boxed{(\sigma_1 - \sigma_2)^2 + (\sigma_2 - \sigma_3)^2 + (\sigma_3 - \sigma_1)^2 = 2\sigma_{yp}^2} \qquad (12\text{-}11)$$

For plane stress, $\sigma_3 = 0$, and Eq. 12-11 in dimensionless form becomes

$$\left(\frac{\sigma_1}{\sigma_{yp}}\right)^2 - \left(\frac{\sigma_1}{\sigma_{yp}}\frac{\sigma_2}{\sigma_{yp}}\right) + \left(\frac{\sigma_2}{\sigma_{yp}}\right)^2 = 1 \qquad (12\text{-}12)$$

This is an equation of an ellipse, a plot of which is shown in Fig. 12-6. Any stress falling within the ellipse indicates that the material behaves elastically. Points on the ellipse indicate that the material is yielding. This is the same interpretation as that given earlier for Fig. 12-4. On unloading, the material behaves elastically.

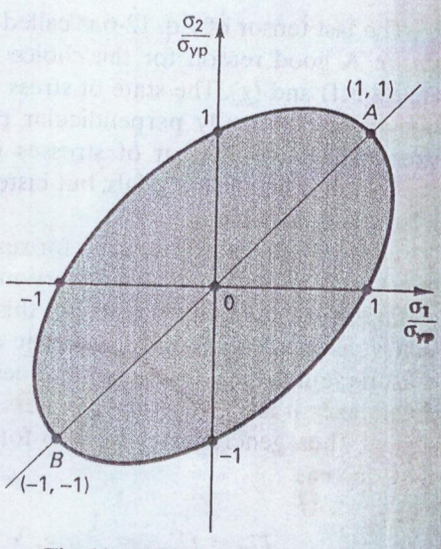

Fig. 12-6 Yield criterion based on maximum distortion energy.

This theory does not predict changes in the material response when hydrostatic tensile or compressive stresses are added. Since only differences of the stresses are involved in Eq. 12-11, adding a constant stress to each does not alter the yield condition. For this reason, in the three-dimensional stress space, the yield surface becomes a cylinder with an axis having all three direction cosines equal to $1/\sqrt{3}$. Such a cylinder is shown in Fig. 12-7(a). The ellipse in Fig. 12-6 is simply the intersection of this cylinder with the σ_1–σ_2 plane. It can also be shown that the yield surface for the maximum shear stress criterion is a hexagon that fits into the tube, shown in Fig. 12-7.

The fundamental relation given by Eq. 12-11 may also be derived by formulating the second invariant, Eq. 11-26, of the deviatoric stresses given by the last matrix in Eq. 12-6. Such an approach is generally favored in the mathematical theory of plasticity. The derivation given before gives greater emphasis to physical behavior. As can be noted from the structure of Eq. 12-11 and the accompanying Figs. 12-6 and 12-7, it is a continuous

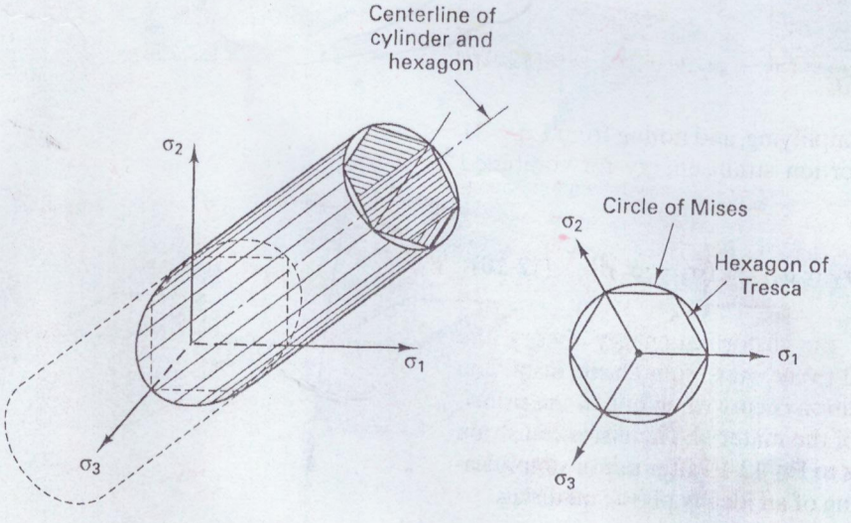

(a) (b) View along the axis of the cylinder

Fig. 12-7 Yield surfaces for triaxial state of stress.

function, making it attractive in analytical and numerical applications. This widely used constitutive equation for perfectly plastic material is often referred to as the *Huber-Hencky-Mises,* or simply the *von Mises, yield condition.*[5]

Both the maximum shear stress and the distortion-energy yield conditions have been used in the study of viscoelastic phenomena under combined stress. Extension of these ideas to strain-hardening materials is also possible. Such topics, however, are beyond the scope of this text.

12-4. Comparison of Maximum-shear and Distortion-energy Theories for Plane Stress

Plane stress problems occur especially frequently in practice and are largely emphasized in this text. Therefore, it is useful to make a comparison between the two most widely used yield criteria for ductile materials for this case. The maximum shear-stress criterion directs its attention to the maximum shear stress in an element. The distortion-energy criterion does this in a more comprehensive manner by considering in three dimensions the energy caused by shear deformations. Since shear stresses are the main parameters in both approaches, the difference between the two is not large. A comparison between them for plane stress is shown in Fig. 12-8. Here the Tresca hexagon for the maximum shear-stress theory and the von Mises ellipse for the maximum distortion-energy theory have the meanings already described. Either one of the lines gives a criterion for yield for a perfectly plastic material. Yield of a material is said to begin whenever either uniaxial or biaxial stresses reach the bounding lines. If a stress point for the principal stresses σ_1 and σ_2 falls within these curves, a material behaves elastically. Since no strain-hardening behavior (see Fig. 2-18) is included in these mathematical models, no stress points can lie outside the curves, as yielding continued as the stress level given by the curves. More advanced theories are not considered in this text.[6]

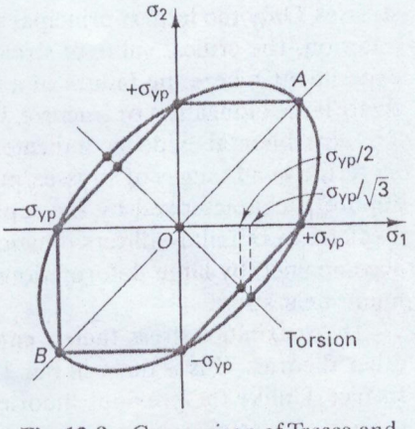

Fig. 12-8 Comparison of Tresca and von Mises yield criteria.

It can be seen from Fig. 12-8 that the discrepancy between the two theories is not very large, the maximum shear-stress theory being in general more conservative. As to be expected, the uniaxial stresses given by both are equal to those corresponding to simple tension or compression. It is assumed that

[5] In the past, this condition has also been referred to as the *octahedral shearing stress theory.* See A. Nadai, *Theory of Flow and Fracture of Solids* (New York: McGraw-Hill, 1950), Vol. 1, or A. P. Boresi and O. M. Sidebottom, *Advanced Mechanics of Materials,* 4th ed. (New York: Wiley, 1985), 18.

[6] K. Washizu, *Variational Methods in Elasticity and Plasticity,* 2nd ed. (New York: Pergamon, 1975); L. E. Malvern, *Introduction to the Mechanics of a Continuous Medium* (Englewood Cliffs: Prentice Hall, 1969).

these basic stresses are of *equal* magnitude. The yield criteria in the second and fourth quadrant indicate smaller strengths at yield than that for uniaxial stresses. The largest discrepancy occurs when two of the principal stresses are equal but of opposite sign. This condition develops, for example, in torsion of thin-walled tubes. According to the maximum shear-stress theory, when $\pm\sigma_1 = \mp\sigma_2$, these stresses at yield can reach only $\sigma_{yp}/2$. The maximum distortion-energy theory limits this stress to $\sigma_{yp}/\sqrt{3} = 0.577\sigma_{yp}$. Points corresponding to these stresses are identified in Fig. 12-8. These values of yield in shear stress are frequently used in design applications.

12-5. Maximum Normal-stress Theory

The maximum normal-stress theory, or simply the maximum stress theory,[7] asserts that failure or fracture of a material occurs when the maximum normal stress at a point reaches a critical value regardless of the other stresses. Only the largest principal stress must be determined to apply this criterion. The critical value of stress σ_{ult} is usually determined in a tensile experiment, where the failure of a specimen is defined to be either excessively large elongation or fracture. Usually, the latter is implied.

Experimental evidence indicates that this theory applies well to *brittle* materials in all ranges of stresses, providing a tensile principal stress exists. Failure is characterized by the separation, or the cleavage, fracture. This mechanism of failure differs drastically from the ductile fracture, which is accompanied by large deformations due to slip along the planes of maximum shear stress.

The maximum stress theory can be interpreted on graphs, as can the other theories. This is done in Fig. 12-9. Failure occurs if points fall on the surface. Unlike the previous theories, this stress criterion gives a bounded surface of the stress space.

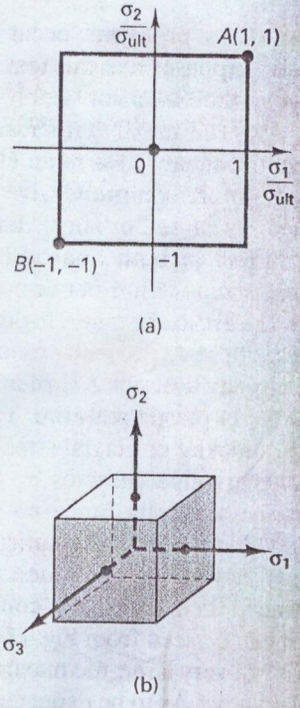

Fig. 12-9 Fracture envelope based on maximum stress criterion.

12-6. Comparison of Yield and Fracture Criteria

Comparison of some classical experimental results with the yield and fracture criteria presented before is shown in Fig. 12-10.[8] Note the particularly good agreement between the maximum distortion-energy theory and

[7]This theory is generally credited to W. J. M. Rankine, an eminent British educator (1820–1872). An analogous theory based on the maximum strain, rather than stress, being the basic criterion of failure was proposed by the great French elastician, B. de Saint-Venant (1797–1886). Experimental evidence does not corroborate the latter approach.

[8]The experimental points shown on this figure are based on classical experiments by several investigators. The figure is adapted from a compilation made by G. Murphy, *Advanced Mechanics of Materials* (New York: McGraw-Hill, 1964), 83.

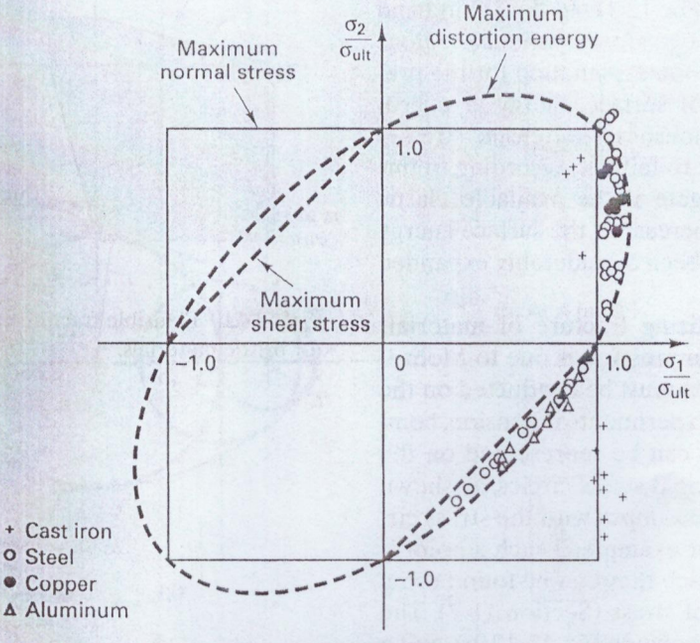

Fig. 12-10 Comparison of yield and fracture criteria with test data.

experimental results for ductile materials. However, the maximum normal-stress theory appears to be best for brittle materials and can be unsafe for ductile materials.

All the theories for uniaxial stress agree since the simple tension test is the standard of comparison. Therefore, if one of the principal stresses at a point is large in comparison with the other, all theories give practically the same results. The discrepancy between the criteria is greatest in the second and fourth quadrants, when both principal stresses are numerically equal.

In the development of the theories discussed before, it has been assumed that the properties of material in tension and compression are alike—the plots shown in several of the preceding figures have two axes of symmetry. On the other hand, it is known that some materials, such as rocks, cast iron, concrete, and soils, have drastically different properties depending on the sense of the applied stress. This is the greatest flaw in applying the classical idealizations to materials having large differences in their mechanical behavior in tension and compression. An early attempt to adopt the maximum shear theory to achieve better agreement with experiments was made by Duguet in 1885.[9] The improved model recognizes the higher strengths of brittle materials in biaxial compression than in tension. Therefore, the region in biaxial tension in the principal stress space is made

[9] A. Nadai, *Theory of Flow and Fracture of Solids* (New York: McGraw-Hill, 1950).

smaller than it is for biaxial compression; see Fig. 12-11. In the second and fourth quadrants, a linear change between the two aforementioned regions is assumed. A. A. Griffith,[10] in a sense, refined the explanation for the previous observations by introducing the idea of surface energy at microscopic cracks and showing the greater seriousness of tensile stresses compared with compressive ones with respect to failure. According to this theory, an existing crack will rapidly propagate if the available elastic strain energy release rate is greater than the increase in the surface energy of the crack. The original Griffith concept has been considerably expanded by G. R. Irwin.[11]

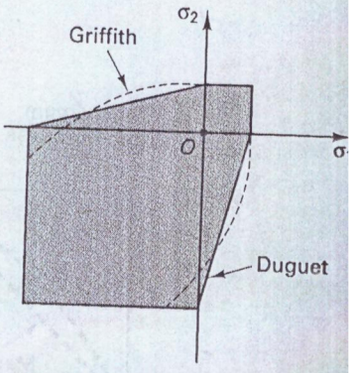

Fig. 12-11 Plausible fracture criteria for brittle materials.

Another important attempt for rationalizing fracture of materials having different properties in tension and compression is due to Mohr.[12] In this approach, several different experiments must be conducted on the same material. For example, if the results of experiments in tension, compression, and shear are available, the results can be represented on the same plot using their respective largest principal stress circles, as shown in Fig. 12-12(a). The points of contact of the *envelopes* with the stress circles define the state of stress at a fracture. For example, if such a point is A (or A'), the stresses and the plane(s) on which they can be found using the established procedure for Mohr's circle of stress (Section 11-7). The corresponding planes for points A or A' are shown in Fig. 12-12(b), and a material such as duraluminum does fracture in tension at a flat angle, as shown. Similarly, by relating the fracture planes to either point B or B', the fracture occurs at a steep angle characteristic of concrete cylinders tested in compression, as in Fig. 12-12(c). Such agreements with experiments support the assumed approach.

The data from Fig. 12-12(a) can be replotted in the principal stress space, as in Fig. 12-12(d). Since in the first quadrant, the *minimum* principal stress $\sigma_3 = 0$, and in the third quadrant, $\sigma_3 = 0$ is the *maximum* principal stress, per Fig. 12-12(a)–(c), in these quadrants the fracture lines in the principal stress space are similar to those of Fig. 12-11. Moreover, if the material strengths in tension and compression are the same, a hexagon identical to that shown in Fig. 12-10 is obtained. However, whereas the hexagon in Fig. 12-10 gives a *yield* condition for *ductile* materials, in the present context it defines a *fracture* criterion for *brittle* materials.

Extrapolation of Mohr envelopes beyond the range of test data is not advisable. In many applications, this may mean that parts of the stress cir-

[10]A. A. Griffith, "The phenomena of rupture and flow of solids," *Philosophical Transactions of the Royal Society of London,* Series A, **221** (1920), 163–198.

[11]G. R. Irwin, "Fracture mechanics," *Proceedings, First Symposium on Naval Structural Mechanics* (Long Island City, NY: Pergamon, 1958), 557. Also see *A Symposium on Fracture Toughness Testing and Its Applications,* American Society for Testing and Materials Special Technical Publication No. 381 (Philadelphia, PA: American Society for Testing and Materials and Washington, DC: National Aeronautics and Space Administration, 1965).

[12]As noted earlier, Otto Mohr was also principally responsible for the development of the stress circle bearing his name.

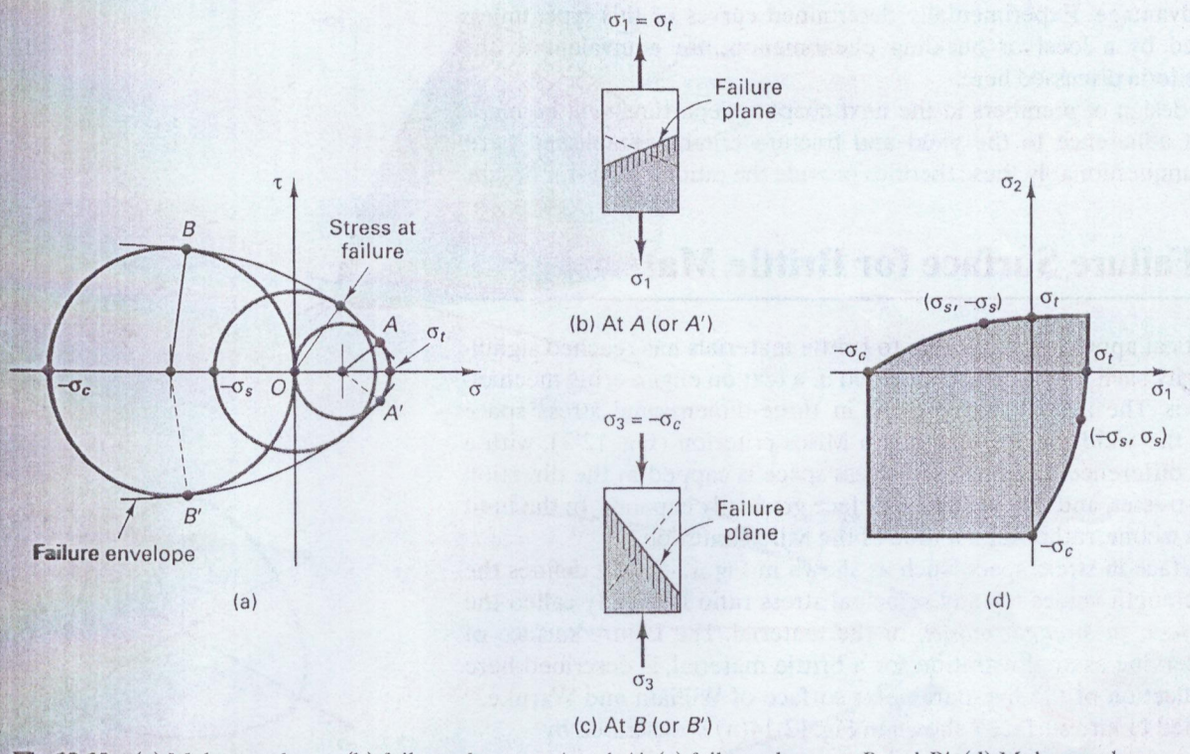

Fig. 12-12 (a) Mohr envelopes, (b) failure planes at A and A', (c) failure planes at B and B', (d) Mohr envelope solution in principal stress space.

cles for tension and compression should be taken as envelope ends. Interpolation along the failure envelopes between these two partial end stress circles is justified, and a stress circle for other conditions can be placed between them. When more extensive data are lacking conservatively, straight-line envelopes can be used.

The use of straight lines for asymptotes has a rational basis and has been found particularly advantageous in soil mechanics. For a loose granular media such as sand, the straight-line Mohr envelopes correspond to the limiting condition of dry friction, $\mu = \tan \phi$; see Fig 12-13. Any circle tangent to the envelope, as at B, gives the state of critical stress. If some cohesion can be developed by the media, the origin O is moved to the right such that at zero stress, the τ intercept is equal to the cohesion. As soils basically cannot transmit tensile stresses, in specialized literature it is customary to direct the compression axis to the right.

Unlike the maximum distortion-energy theory, the fracture theory based on Mohr envelopes, using the largest principal stress circles, neglects dependence on the intermediate principal stress.

Sometimes the yield and fracture criteria discussed before are inconvenient to apply. In such cases, interaction curves such as in Fig. 9-16 can be

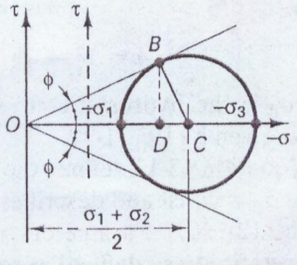

Fig. 12-13 Mohr envelopes for cohesionless granular media.

used to advantage. Experimentally determined curves of this type, unless complicated by a local or buckling phenomenon, are equivalent to the strength criteria discussed here.

In the design of members in the next chapter, departures will be made from strict adherence to the yield and fracture criteria established here, although, unquestionably, these theories provide the rational basis for design.

12-7. Failure Surface for Brittle Materials

The analytical approach applicable to brittle materials has reached significant maturity such that it can be included in a text on engineering mechanics of solids. The available treatment in three-dimensional stress space resembles the yield surface of the von Mises criterion (Fig. 12-7), with a significant difference. The enclosed stress space is capped in the direction of tensile stresses, and the enclosing surface gradually expands. In the limit it becomes a cone, rather than a tube of the Mises criterion.

The surface in stress space, such as shown in Fig. 12-7, that defines the ultimate strength values for any principal stress ratio is usually called the *failure surface,* or *strength model,* of the material. The failure surface of concrete, serving as an illustration for a brittle material, is described here by a modification of the five-parameter surface of William and Warnke.[13] The modified failure surface[14] shown in Fig. 12-14(a) is described by

$$\tau_0(\sigma_0, \theta) = \tau_c \frac{a\eta + b\sqrt{a(\eta^2 - 1) + b^2}}{a\eta^2 + b^2} \tag{12-13}$$

where

$$a = \tau_c^2 - \tau_t^2; \quad b = 2\tau_t - \tau_c; \quad \eta = 2\cos\theta \tag{12-14}$$

and σ_0 is the hydrostatic stress, defined in Eq. 11-31, and θ is the Lode angle, given by Eq. 11-29.

Equation 12-13 defines the form of the failure surface in the deviatoric plane $\sigma_0 = \text{const}$ and describes a smooth convex (elliptical) curve depicted in Fig. 12-14(b). Parameters τ_c and τ_t in Eq. 12-14 are functions of the hydrostatic stress, defined as roots of the quadratic equations

$$\tau_c^2 + A\left(\frac{\tau_c}{\sqrt{2}} + \sigma_0\right) + B = 0 \tag{12-15}$$

$$\tau_t^2 + A\left(\frac{\tau_t}{\sqrt{2}}\beta + \sigma_0\right) + B = 0 \tag{12-16}$$

[13]See K. J. William and E. P. Warnke, "Constitutive model for the triaxial behavior of concrete," *Int. Association for Bridge and Struct. Engrg. Proc.,* **19**, (1975), 1–30.

[14]See T. A. Balan, F. C. Filippou, and E. P. Popov, "Constitutive model for 3D cyclic analysis of concrete structures," *J. Engrg. Mechanics, ASCE,* **123**, no. 2 (February 1997), 143–153.

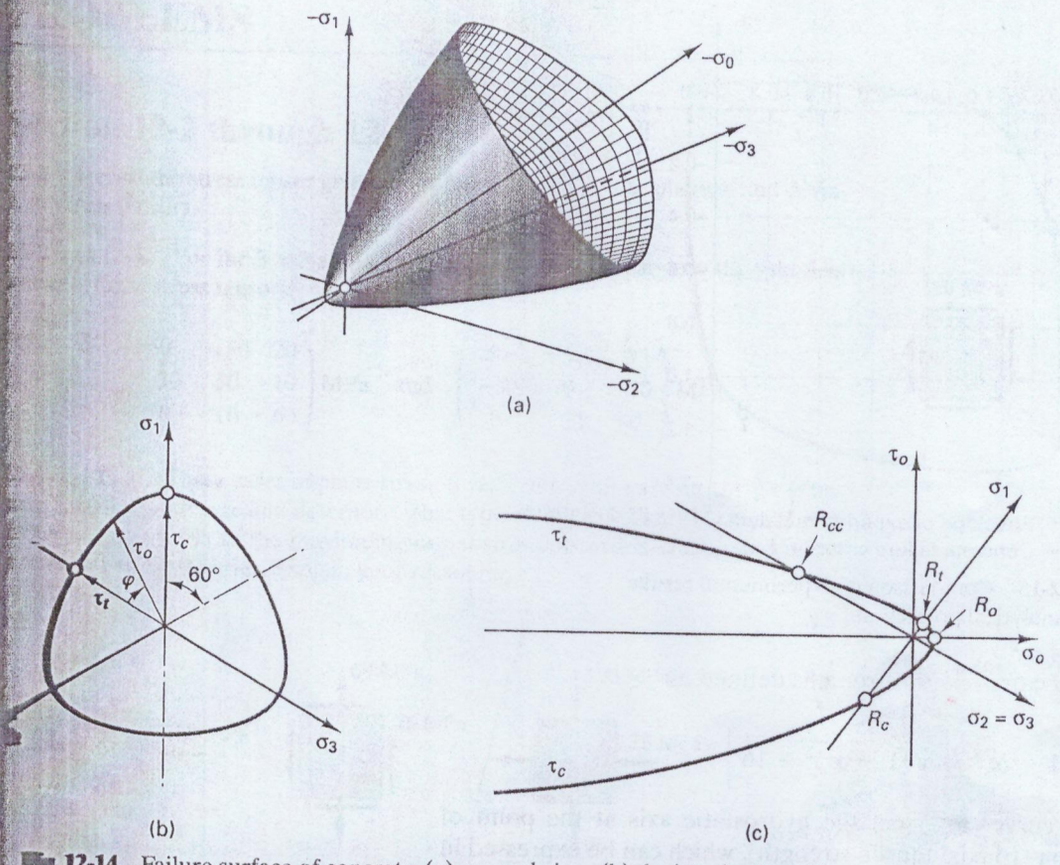

Fig. 12-14 Failure surface of concrete: (a) general view; (b) deviatoric view; (c) meridianal view.

$$A = \frac{R_c}{9\alpha}(1 - \alpha^2)(2 + \alpha); \quad B = -\frac{2}{9}R_c^2 \tag{12-17}$$

$$\alpha = \frac{R_t}{R_c}; \quad \beta = \frac{4 - \alpha}{2 + \alpha} \tag{12-18}$$

R_c, R_t are the uniaxial compression and tensile strengths, respectively. It should be noted that Eqs. 12-15 and 12-16 represent the compression ($\theta = 60°$) and the tension ($\theta = 0°$) meridians of the material failure surface. On the plane $\sigma_2 = \sigma_3$ (sometimes called the Rendulic plane), as can be seen in Fig. 12-14(c), the meridianal sections are the parabolic curves, which pass through a set of characteristic points that define the following strength parameters of the material:

R_c, R_t = uniaxial compression and tensile strengths, respectively

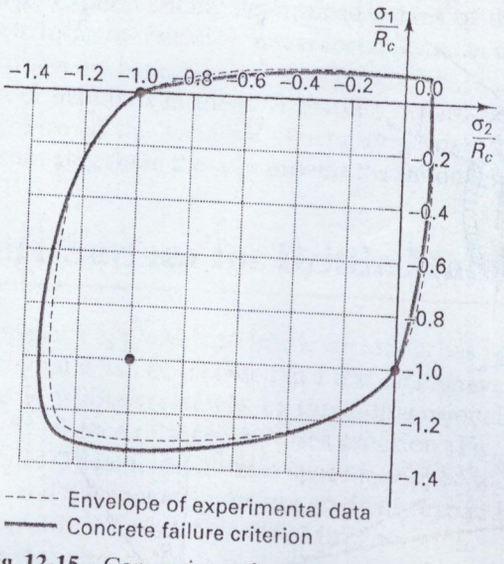

Fig. 12-15 Comparison of experimental results with analytical prediction.

R_{cc} = biaxial compression strengths defined as

$$R_{cc} = \frac{R_c}{4}\left[(1-\alpha^2) + \sqrt{(1-\alpha^2)^2 + 16}\right]$$

The meridianal curves intersect the hydrostatic axis at the point of equitriaxial extension (triaxial tensile strength), which can be expressed in terms of uniaxial compression and tensile strength as

$$R_0 = -\frac{B}{A} = \frac{2R_t}{(1-\alpha^2)(2+\alpha)}$$

In Fig. 12-15 the material strength predicted by the failure surface is compared with plane stress experimental data.[15] The particular concrete was calibrated by the following strength parameters: $R_c = 32.1$ MPa (4.66 ksi) and $R_t = 3.1$ MPa (0.45 ksi). The resulting failure trace of the strength model in plane $\sigma_3 = 0$ provides very close agreement with considered experimental data.

Careful recent experimental research on concrete specimens of different strengths strongly corroborates this approach. This work now has been extended to include strain-hardening effects and has been implemented for use with a computer.[16]

[15]Adopted from H. Kupfer, H. K. Hilsdorf, and H. Rusch, "Behavior of concrete under biaxial stresses," *ACI J.*, **66**, no. 8 (1969), 656–666.

[16]C. Bedard and M. D. Kostovos, "Application of NLFEA to concrete structures," *J. Struct. Div.* ASCE, **111** (ST12) (1985); Z. P. Bažant, ed., *Mechanics of Geomaterials: Rocks, Concrete, Soils* (Chichester: Wiley, 1985).